

# The use of DAPI fluorescence lifetime imaging for investigating chromatin condensation in human chromosomes

Ana Katrina Estandarte<sup>1,2\*</sup>, Stanley Botchway<sup>2,3</sup>, Christophe Lynch<sup>1,2</sup>, Mohammed Yusuf<sup>1,2</sup> and Ian Robinson<sup>1,2</sup>

<sup>1</sup> London Centre for Nanotechnology, University College London, London, WC1H 0AH, UK

<sup>2</sup> Research Complex at Harwell, Rutherford Appleton Laboratory, Oxon, OX11 0FA, UK

<sup>3</sup> Science and Technology Facilities Council, Rutherford Appleton Laboratory, Oxon, OX11 0QX, UK

\* To whom correspondence should be addressed. Tel: +44(0)1235567847; Fax: +44(0)1235567799; Email: ana.estandarte.11@ucl.ac.uk

## Abstract

The characteristic chromatin condensation of human chromosomes was followed by fluorescence lifetime imaging microscopy (FLIM), a technique which utilizes a fluorophore's lifetime to probe changes in its environment. Human metaphase and interphase chromosomes were labeled with the DNA minor groove binder, DAPI, followed by measurement and imaging of the excited state lifetime using multiphoton excitation. DAPI excited state lifetime variations in metaphase chromosome spreads showed differentially compacted regions of chromatin along the length of the chromosomes. The heteromorphic regions of chromosomes 1, 9, 15, 16, and Y, which consist of highly condensed constitutive heterochromatin, showed statistically significant shorter DAPI lifetime values than the rest of the chromosomes. Differences in the DAPI lifetimes for the heteromorphic regions suggest differences in the structures of these regions. DAPI lifetime variations across an interphase nucleus showed variation in chromatin compaction in interphase and formation of chromosome territories within the nucleus.

## Introduction

The packaging of cellular nuclear DNA into chromosomes, particularly at the nanometer length scales and the consequences thereof, is still little understood. Knowledge of the physical state of the genetic material of the cell, the form and subsequent function of the substructure of chromosomes during its transcription and replication, and during cell division, is highly desirable. Chromosomes are composed of chromatin, a complex of DNA and proteins, which are arranged into elementary structural units of nucleosomes. Each nucleosome consists of 147 base pairs of DNA wrapped around a core of eight histone proteins (1). These nucleosomes are arranged into 11-nm fibers having a “beads-on-a-string”

appearance (2). As the cell cycle proceeds from interphase to metaphase, the chromatin undergoes further condensation by the addition of a protein scaffold thus forming higher order structures until the chromosomes reach the metaphase stage of mitosis, their most compact state (3). The organization of chromatin into these higher-order structures and the factors that play a role in the condensation process remains a subject of debate and represent one of the key challenges in structural biology.

Chromatin has been historically categorized into two structural states: heterochromatin and euchromatin (4). Heterochromatin has been described as the chromatin fraction that is more compact and remains condensed throughout the cell cycle except during its replication. It is thought to be inactive in transcription, has a low gene density, and is replicated late in the S-phase (5, 6). It can be further classified into constitutive heterochromatin, which is composed of repetitive sequences of DNA known as satellite repeats and is associated mostly with pericentromeric and telomeric regions of the chromosome, and facultative heterochromatin, which can interconvert between heterochromatic and euchromatic states when triggered by several factors such as acetylation and methylation (7, 8). Whilst euchromatin has been described as the chromatin fraction that is relatively decompacted and decondenses during interphase, it is active in transcription, more likely to contain genes, and is replicated early in S-phase (5, 6).

Visualization of subchromosomal regions can be achieved through so-called banding, a characteristic striped appearance that results from the differential staining along the length of a chromosome. Bands also allow the identification of individual chromosomes and the presence of possible abnormalities therein such as deletions, insertions, and translocations and are used in cytogenetic clinical laboratories. The common banding patterns observed are G-, R-, and C- banding patterns (9). Usually, the contrast between the bands is based on the relative intensity of the stain.

A vital characteristic of a fluorophore apart from excitation, emission wavelength, and intensity is its fluorescence excited state lifetime ( $\tau$ ), which can be defined as the average time a fluorophore stays in the electronic excited state. There are different pathways of relaxation (e.g. internal conversion, dynamic quenching, energy transfer) for a fluorophore in the excited state aside from fluorescence which can all compete kinetically with fluorescence and thereby affect the fluorescence rate (10). The rates of these relaxation pathways are

sensitive to many factors such as proximity of the fluorophore to other fluorophores and quenching species, and dielectric constant of the medium. Hence, fluorescence lifetime can change markedly depending on a fluorophore's environment.

Fluorescence lifetime imaging microscopy (FLIM) is a technique that maps the spatial arrangement of lifetime and can act as a probe to changes in the fluorophore's environment. A lifetime image is acquired wherein the fluorescence lifetime is measured, with temporal resolution of nanoseconds or less, at every pixel of the image. FLIM has many applications across both physical and life sciences. It is widely used for investigations at Förster resonance energy transfer (FRET) lengths (1-10 nm) between a fluorophore and another molecule to probe distances and study interactions between molecules (e.g. homo- and hetero-dimerisations and protein-protein interactions (11, 12)). A major advantage of FLIM over intensity-based fluorescence imaging is that, whereas fluorescence intensity is dependent upon a variety of instrumental and sample influences, such as variations of fluorophore concentration and photobleaching, fluorescence lifetime is generally independent of variations in these factors (13).

Little is known about the sensitivity of fluorescence lifetime to changes in chromosome environment. In this work, FLIM is used to investigate the different chromosome substructures at the nanometer length scales by the variations in the DAPI (4'-6-diamidino-2-phenylindole) excited state lifetime in DAPI-stained human metaphase chromosomes and interphase nucleus. DAPI is a nucleic-acid specific fluorophore that is widely used in chromosome staining because of its high quantum yield ( $\phi_f = 0.92$ ) when bound to DNA (14), and high photostability. The  $\phi_f$  of unbound DAPI (0.04) is several orders of magnitude less than in the presence of DNA. Here we observed variations in the DAPI excited state lifetime along the length of the metaphase chromosomes and across the interphase nucleus, reflecting differentially compacted regions of chromatin. The pericentromeric regions of chromosomes 1, 9, and 16, short arm of chromosome 15, and distal region of chromosome Y in the metaphase spreads showed significantly shorter lifetime values ( $\tau_{1,16,Y} = 2.57 \pm 0.06$  ns,  $\tau_{9a,15} = 2.41 \pm 0.06$  ns, and  $\tau_{9b} = 2.21 \pm 0.05$  ns) as compared with the rest of the chromosomes ( $\tau = 2.80 \pm 0.09$  ns).

## **Results**

### **Excited State Characteristics of DAPI in Solution**

The lifetime of unbound DAPI in PBS solution (pH 7.2) was initially measured to determine both the sensitivity of the system as well as the accuracy of lifetime measurements since the excited state lifetime of DAPI is known (15). The fluorescence decay showed a double exponential character. The relative amplitudes of the long and short lifetime components were determined to be 0.41 and 0.59, respectively. The value of the long lifetime component, 2.66 ns, agrees well with literature while the value of the short lifetime component, 0.36 ns, is higher than that described in the literature at pH 7 where the value range is 0.19-0.24 ns (15).

### **FLIM of DAPI Bound to Metaphase Chromosomes**

The fluorescence decay of DAPI bound to human metaphase chromosomes was found to have single exponential characteristics. This is in contrast to the double exponential fluorescence decay found for unbound DAPI in solution.

Figure 1 shows a lifetime image of a typical chromosome spread. False color is used to represent the lifetime value at each image pixel. The lifetime images show that there is a variation in the lifetime of DAPI along the length of the chromosomes. The DAPI fluorescence decay curves with normalized intensities is also presented in the figure to complement the lifetime images and show that the fluorescence of the DAPI molecules in the red regions has a faster decay than that in the blue regions. The mean lifetime  $\pm$  standard deviation (SD) of DAPI for the measured chromosome spread in Figure 1a was determined to be  $2.91 \pm 0.12$  ns.

### **Identification of Heteromorphic Regions in Chromosomes**

12 chromosome spreads with 45 or 46 chromosomes each were measured from three slides. The lifetime images and lifetime distribution curves of these spreads show that certain chromosomes have specific regions along their lengths that have significantly short lifetimes, mostly in close proximity to the centromeres.

Figure 2a shows a lifetime image of one of the spreads. The lifetime distribution curves with normalized frequencies for the short lifetime regions (red regions in Figure 2a) and the rest of the chromosomes are shown in Figure 2b. The mean lifetime of DAPI for the short lifetime

regions for the spread in Figure 2a was determined to be  $2.48 \pm 0.13$  ns while that for the rest of the chromosomes in the spread was determined to be  $2.80 \pm 0.09$  ns.

mFISH was performed in all of the measured spreads in order to identify the chromosomes containing the short lifetime regions. The mFISH image and karyotype of the spread in Figure 2a are shown in Figures 2c and 2d, respectively. The regions showing shorter lifetimes, as compared with the rest of the chromosomes, in all of the measured spreads were identified to be the pericentromeric regions of chromosomes 1, 9, and 16, the short arm of chromosome 15, and the distal region of chromosome Y. These regions are generally classified as heteromorphous regions.

To further characterise the heteromorphous regions, Table 1 shows the mean lifetime value of DAPI for each of the heteromorphous regions in Figure 2a. Since each chromosome number consists of a pair of chromosomes, the mean lifetimes and standard deviations for the heteromorphous regions obtained for chromosomes with the same chromosome number were averaged and pooled, respectively.

It can be observed from the table that the measured lifetimes for the heteromorphous regions of chromosomes 1, 16, and Y are similar and are significantly longer than that of chromosomes 9 and 15. The heteromorphous region of chromosome 9 can be described by two lifetimes so that region 9a has a similar value to that of chromosome 15 while region 9b has a shorter lifetime than that of region 9a. The other measured spreads (Supplementary Tables 1-11) show a similar trend of the heteromorphous regions of chromosomes 9 and 15 having shorter lifetimes than that of chromosomes 1, 16, and Y.

### **Trends in DAPI Lifetime with Chromosome Area**

Chromosomes prepared for this study were blocked in metaphase using colcemid; cells in the synchronized population are not all expected to be exactly in the same stage of the cell cycle and will therefore display different degrees of chromatin compaction depending on which time they reached the metaphase checkpoint relative to other cells in the population. This variation in the compaction is reflected by a variation in the relative area of a particular chromosome from one chromosome spread to another on the same slide. In order to observe the effect of the different states of compaction on the fluorescence lifetime, we correlated the mean DAPI lifetimes for various examples of chromosome 1's from one slide and their

heteromorphous regions with the measured chromosome area. Analysis of the heteromorphous regions and calculation of the chromosome areas were carried out using the Avizo software. The lifetime value at each pixel of the chromosome images was given a false color depending on the lifetime range of the spreads. The red regions, which represent the low lifetime values, were identified as the heteromorphous regions. Again, the lifetime values for chromosome pairs were averaged.

The graph in Figure 3 shows that the mean lifetimes of DAPI for chromosome 1 and its heteromorphous region decrease strongly with decreasing chromosome 1 area. To the extent to which the area of a chromosome in a spread represents packing density, the observed trend suggests a linear dependence on density, representing the degree of condensation. A similar trend is also observed for chromosome spreads on another slide (Supplementary Fig. 1).

### **Effect of DAPI Concentration on Lifetime**

Metaphase chromosomes stained with a higher concentration of DAPI were also measured to investigate possible different binding sites of DAPI in DNA and how this can affect the lifetime. A double exponential character was observed for the DAPI fluorescence decay. The lifetime images (Supplementary Fig. 2) show that there is a variation in both the short and long lifetime components along the length of the chromosomes and this variation correlates so that the value of the long lifetime component decreases as the value of the short component decreases. The mean lifetimes  $\pm$  SD of DAPI for the first and second components were calculated to be  $1.06 \pm 0.04$  ns and  $3.45 \pm 0.05$  ns, respectively.

### **FLIM of DAPI Bound to Interphase Chromosomes within the Nucleus**

The excited state lifetime of DAPI bound to interphase chromosomes within a nucleus was also imaged, as shown in Figure 4. A single exponential character was observed for the DAPI fluorescence decay. The lifetime images of the measured nucleus show that there is a strong variation in the DAPI lifetime across the interphase nucleus. Moreover, the images show blocks of short lifetime values inside the nucleus.

A z-stack of the nucleus was taken using a multiphoton excitation (at 760nm) confocal microscope. Figures 4a and 4c show images obtained at  $-0.50 \mu\text{m}$  and  $+0.50 \mu\text{m}$ , respectively, from the original focal plane (Figure 4b). Even though the fixed nucleus is highly collapsed from its native spherical shape as a result of the fixation process, this shows

the locations of the blocks in three dimensions. 3D reconstruction of the confocal z-stack images (Supplementary Fig. 4) and quantitative analysis of the blocks were carried out using the Avizo software.

Table 2 shows the volume, mean lifetime, and position, in relation to the radius of the nucleus, of the heterochromatic blocks. It can be observed from the table that the heterochromatic blocks are located either near the periphery of the nucleus or halfway between the center and periphery of the nucleus. No blocks of very short lifetime values are observed close to the center of the nucleus. The calculated volumes for these blocks are found to be larger than the typical volume of a chromosome ( $\sim 1-3 \text{ um}^3$ ), suggesting a considerable spreading in interphase. The error in the volume calculations could be due to a poor z-calibration of the confocal microscope during the measurements or that the multiphoton volume is larger than that of the confocal at times. We examined three nuclei in this study and found that all showed a similar distribution of short lifetime regions (Supplementary Figs. 5 and 6).

## **Discussion**

The two lifetime components observed for unbound DAPI in solution may be due to ground-state heterogeneity arising from two differentially solvated populations of DAPI (16). The indole ring of one of the populations is preferentially solvated in the ground-state, allowing intramolecular proton transfer, from the 6-amidinium group of DAPI to the NH of the indole ring, to take place in the excited state. The proton transfer process competes with fluorescence and results in a non-fluorescent species thus accounting for the short lifetime component observed. The long lifetime component arises from the population where proton transfer at the indole ring does not occur in the excited state. The stability of these two differentially solvated populations depends on the different rotamers of DAPI either at the C6 of the indole ring or at the C2 (17).

The lifetime images of DAPI-stained human metaphase chromosomes showed that there is a variation in the lifetime of DAPI along the length of the chromosomes. The observed variation in lifetime may be a reflection of the sensitivity of lifetime to the differentially compacted regions of chromatin (i.e. heterochromatin and euchromatin) along the chromosome length. The mean lifetime of DAPI for the measured chromosome spread in Figure 1a is not too dissimilar to the long lifetime component of unbound DAPI in PBS

buffer thus signifying protection of the DAPI molecules from solvent quenching upon binding to the chromosomes. DAPI binds to the chromosomes through the minor groove of the DNA at the AT-rich regions (18, 19). Upon binding, it enters a hydrophobic environment thus preventing intramolecular proton transfer. Furthermore, the -NH functional group of the DAPI's indole ring becomes unavailable for the transfer as it forms a hydrogen bond with the thymine oxygen of the DNA.

The regions showing significantly short lifetimes along the length of the chromosomes were identified to be the heteromorphic regions of chromosomes 1, 9, 15, 16, and Y. Heteromorphic regions are microscopically visible regions on chromosomes that are variable in size, morphology, and staining properties in different individuals (20). They are made up of highly condensed constitutive heterochromatin and consist mostly of satellite DNA. Several studies have suggested that the presence and sequence composition of satellite DNA in constitutive heterochromatin is related to its highly condensed nature (7, 21, 22). Miller et al. (22) has shown that DNA methylation occurs only in certain classes of repetitive DNA and that the heteromorphic regions of chromosomes 1, 19, 15, 16, and Y are intensely methylated. DNA methylation is one of the factors that play a role in the condensed structure of heterochromatin (7, 21, 22). In addition, Dillon et al. (7) has suggested that the pairing between repeats lead to higher-order structures in constitutive heterochromatin.

Since we have also identified a strong correlation between condensation state and lifetime in Fig 3, we therefore suggest that these properties account for the shorter lifetimes observed at the heteromorphic regions. Due to the highly condensed nature of the constitutive heterochromatin, the excited state DAPI molecules can undergo more interactions such as collisions with the DNA bases or other DAPI molecules (23) within these regions thus resulting in the quenching of the DAPI fluorescence. This mechanism could explain why the regions showing shorter lifetimes in the FLIM images correspond to more condensed regions of the chromosomes.

The shorter DAPI lifetimes observed for the heteromorphic regions of chromosomes 9 and 15 as compared with those of the other heteromorphic regions suggest that there is a difference in the structure of the heteromorphic regions of chromosomes 9 and 15 making these regions more condensed than the other heteromorphic regions. This difference in the structures of the heteromorphic regions among the chromosomes may result from a difference in the type and

amount of satellite DNA in these regions. The heteromorphic region of chromosome 9 contains the bulk of the human satellite DNA (24). Hence, the high concentration of satellite DNA in this region may lead to a more condensed structure, which may account for the very short lifetimes observed at this region, especially in region 9b, as compared with that of the other heteromorphic regions. Furthermore, it was shown by Gosden et al. (24) and Jones et al. (25) that human satellite III DNA concentrates mostly at the heteromorphic regions of chromosomes 9 and 15 while human satellite II DNA concentrates mostly at the heteromorphic regions of chromosomes 1, 16, and Y. Chromosome 9 was found to consist of satellite II also but in less concentration. The difference between satellites III and II is that satellite III has more sequence divergence than satellite II thus suggesting that satellite III is older in evolution than satellite II (25, 26). This difference may be one of the factors that lead to the difference in the structures of the heteromorphic regions.

The correlation of the mean lifetimes of DAPI for various chromosome 1's from one slide and their heteromorphic regions with the measured chromosome area shown in Figure 3 confirms the sensitivity of the DAPI fluorescence lifetime with chromatin compaction and demonstrates that in general shorter lifetimes are associated with more condensed chromosomes. Moreover, this result qualitatively agrees with our observation that the highly condensed heteromorphic regions of the chromosomes showed shorter lifetimes than the rest of the chromosomes and support the statement that the longer lifetimes observed along the length of the chromosomes correspond to the less condensed regions of the chromosomes.

The lifetime images of human metaphase chromosomes stained with a higher concentration of DAPI showed the presence of two lifetime components. This may be due to the presence of two different binding modes of DAPI at higher DAPI loading. It has been suggested that DAPI preferentially binds to the minor groove of DNA at the AT-rich regions (18, 19). However, at a high concentration of DAPI where the AT-rich regions become fully saturated, DAPI may also start to bind at the GC-rich regions through external binding (27, 28), where DAPI may undergo electrostatic interaction with the phosphate groups of DNA, or through intercalation (29, 30). These different binding modes can cause different DAPI lifetimes due to different extents of protection of DAPI from solvent quenching. It has been shown that DAPI bound to poly(d(A-T)) through the minor groove to give a longer lifetime (~4 ns) than that of DAPI bound to poly(d(G-C)) through external binding or intercalation (~0.25 ns) (16, 31). This is because DAPI is more protected from solvent quenching when it is bound

through the minor groove than when it is intercalated or bound externally. Furthermore, in the intercalative mode, DAPI can have electronic interaction with the DNA base pairs which then contributes to the quenching of its fluorescence. Hence, the longer lifetime component observed for the chromosomes, used in the quantitative analysis of our data, can be attributed to minor groove binding while the shorter lifetime component can be attributed to external binding and/or intercalation. The lifetime could also report on the physical state of the DNA, such as its degree of supercoiling. Although we cannot completely rule out static DAPI-DAPI quenching in the reduced lifetime data since the excitation and emission of the DAPI fluorescence shows a 10% overlap. It is possible that given the correct dipole moment orientation, homo-dimer energy transfer may occur.

Furthermore, the variations in the DAPI lifetime along the length of the chromosomes observed for both the short and long lifetime components signify that the lifetime variations along the length of the chromosomes observed at low DAPI concentration are not due to different binding modes of DAPI but relate to the chromosome structure. Both lifetime components appear to show a similar relationship between chromatin compaction and lower lifetime values.

The variations in the DAPI lifetime observed across the interphase nucleus reflect differentially compacted chromatin within the nucleus. From our chromosome data and observations, we suggest that the reduced excited state lifetime regions inside the nucleus consist of blocks of highly condensed heterochromatin and may correspond to the heteromorphic regions observed for the metaphase chromosomes. The calculated positions of these heterochromatic blocks agree with several studies performed on the formation of chromosome territories inside an interphase nucleus (32-36). For a spherical interphase nucleus, there is a correlation between the radial positioning of the chromosomes inside the nucleus and the gene density of the chromosomes (32, 33). The late-replicating and gene-poor chromosomes, such as chromosomes 9 and Y, are preferentially located near the periphery of the nucleus. As mentioned earlier, chromosomes 1, 9, 15, 16, and Y contain most of these heterochromatic blocks. Even though chromosomes 1 and 16 are not preferentially located near the periphery of the nucleus because of their high gene density, their heterochromatic blocks, which are late-replicating and gene-poor, tend to position near the periphery (32, 34-36).

Overall, we have shown in this study that FLIM can be effectively used to probe chromosome structure and map out locations of differentially compacted regions of chromatin within the chromosomes.

### **Acknowledgments**

This work was supported by a BBSRC Professorial Fellowship, grant number BB/H022597/1.

### **Supplementary Materials**

Tables 1 to 11

Figures 1 to 6

### **References**

1. Richmond, T. J., and C. A. Davey. 2003. The structure of DNA in the nucleosome core. *Nature* 423:145-150.
2. Finch, J., and A. Klug. 1976. Solenoidal model for superstructure in chromatin. *Proceedings of the National Academy of Sciences* 73:1897-1901.
3. Laemmli, U., S. Cheng, K. Adolph, J. Paulson, J. Brown, and W. Baumbach. 1978. Metaphase chromosome structure: the role of nonhistone proteins. In *Cold Spring Harbor symposia on quantitative biology*. Cold Spring Harbor Laboratory Press. 351-360.
4. Heitz, E. 1928. Das Heterochromatin der Moose, 1. *Jahrb. Wiss. Bot.* 69:762-818.
5. Craig, J. M., and W. A. Bickmore. 1993. Genes and genomes: Chromosome bands—flavours to savour. *Bioessays* 15:349-354.
6. Comings, D. E. 1978. Mechanisms of chromosome banding and implications for chromosome structure. *Annual review of genetics* 12:25-46.
7. Dillon, N., and R. Festenstein. 2002. Unravelling heterochromatin: competition between positive and negative factors regulates accessibility. *TRENDS in Genetics* 18:252-258.
8. Trojer, P., and D. Reinberg. 2007. Facultative heterochromatin: is there a distinctive molecular signature? *Molecular cell* 28:1-13.
9. Jacobs, P. A., and D. S. H. P. Klinger. 1972. Paris conference (1971): Standardization in human cytogenetics. *Cytogenet Genome Res* 11:313-362.
10. Periasamy, A., and R. Clegg. 2010. *FLIM Microscopy in Biology and Medicine*. Chapman & Hall/CRC, USA.
11. Gadella, T., and T. M. Jovin. 1995. Oligomerization of epidermal growth factor receptors on A431 cells studied by time-resolved fluorescence imaging microscopy. A stereochemical model for tyrosine kinase receptor activation. *The Journal of cell biology* 129:1543-1558.
12. Bastiaens, P., and T. M. Jovin. 1996. Microspectroscopic imaging tracks the intracellular processing of a signal transduction protein: fluorescent-labeled protein kinase C beta I. *Proceedings of the National Academy of Sciences* 93:8407-8412.
13. Rost, F. 1992. *Fluorescence Microscopy*. Cambridge University Press, Cambridge, UK.
14. Kapuscinski, J. 1995. DAPI: a DNA-specific fluorescent probe. *Biotechnic & Histochemistry* 70:220-233.
15. Barcellona, M., and E. Gratton. 1991. A molecular approach to 4',6-diamidino-2-phenylindole (DAPI) photophysical behaviour at different pH values. *Biophysical chemistry* 40:223-229.

16. Barcellona, M., and E. Gratton. 1990. The fluorescence properties of a DNA probe. *European Biophysics Journal* 17:315-323.
17. Mazzini, A., P. Cavatorta, M. Iori, R. Favilla, and G. Sartor. 1992. The binding of 4', 6-diamidino-2-phenylindole to bovine serum albumin. *Biophysical chemistry* 42:101-109.
18. Manzini, G., M. Barcellona, M. Avitabile, and F. Quadrifoglio. 1983. Interaction of diamidino-2-phenylindole (DAPI) with natural and synthetic nucleic acids. *Nucleic acids research* 11:8861-8876.
19. Kubista, M., B. Aakerman, and B. Norden. 1987. Characterization of interaction between DNA and 4', 6-diamidino-2-phenylindole by optical spectroscopy. *Biochemistry* 26:4545-4553.
20. Wyandt, H. E., and V. S. Tonk. 2003. *Atlas of Human Chromosome Heteromorphisms*. Springer.
21. Tagarro, I., A. M. Fernández-Peralta, and J. J. González-Aguilera. 1994. Chromosomal localization of human satellites 2 and 3 by a FISH method using oligonucleotides as probes. *Human genetics* 93:383-388.
22. Miller, O. J., W. Schnedl, J. Allen, and B. F. Erlanger. 1974. 5-Methylcytosine localised in mammalian constitutive heterochromatin. *Nature* 251:636-637.
23. Barcellona, M. L., and E. Gratton. 1996. Torsional dynamics and orientation of DNA-DAPI complexes. *Biochemistry* 35:321-333.
24. Gosden, J., A. Mitchell, R. Buckland, R. Clayton, and H. Evans. 1975. The location of four human satellite DNAs on human chromosomes. *Experimental cell research* 92:148-158.
25. Jones, K., J. Prosser, G. Corneo, and E. Ginelli. 1973. The chromosomal location of human satellite DNA III. *Chromosoma* 42:445-451.
26. Corneo, G., E. Ginelli, and E. Polli. 1971. Renaturation properties and localization in heterochromatin of human satellite DNA's. *Biochimica et Biophysica Acta (BBA)-Nucleic Acids and Protein Synthesis* 247:528-534.
27. Barcellona, M., R. Favilla, J. Von Berger, M. Avitabile, N. Ragusa, and L. Masotti. 1986. DNA-4', 6-diamidino-2-phenylindole interactions: A comparative study employing fluorescence and ultraviolet spectroscopy. *Archives of biochemistry and biophysics* 250:48-53.
28. Cavatorta, P., L. Masotti, and A. Szabo. 1985. A time-resolved fluorescence study of 4', 6'-diamidino-2-phenylindole dihydrochloride binding to polynucleotides. *Biophysical chemistry* 22:11-16.
29. Wilson, W. D., F. A. Tanious, H. J. Barton, R. L. Jones, L. Strekowski, and D. W. Boykin. 1989. Binding of 4', 6-diamidino-2-phenylindole (DAPI) to GC and mixed sequences in DNA: intercalation of a classical groove-binding molecule. *Journal of the American Chemical Society* 111:5008-5010.
30. Trotta, E., E. D'Ambrosio, G. Ravagnan, and M. Paci. 1995. Evidence for DAPI intercalation in CG sites of DNA oligomer [d (CGACGTCG)]<sub>2</sub>: a <sup>1</sup>H NMR study. *Nucleic acids research* 23:1333-1340.
31. Barcellona, M. L., and E. Gratton. 1989. Fluorescence lifetime distributions of DNA-4', 6-diamidino-2-phenylindole complex. *Biochimica et Biophysica Acta (BBA)-General Subjects* 993:174-178.
32. Boyle, S., S. Gilchrist, J. M. Bridger, N. L. Mahy, J. A. Ellis, and W. A. Bickmore. 2001. The spatial organization of human chromosomes within the nuclei of normal and emerin-mutant cells. *Human molecular genetics* 10:211-219.

33. Tanabe, H., F. A. Habermann, I. Solovei, M. Cremer, and T. Cremer. 2002. Non-random radial arrangements of interphase chromosome territories: evolutionary considerations and functional implications. *Mutation Research/Fundamental and Molecular Mechanisms of Mutagenesis* 504:37-45.
34. Ferreira, J., G. Paoletta, C. Ramos, and A. I. Lamond. 1997. Spatial organization of large-scale chromatin domains in the nucleus: a magnified view of single chromosome territories. *The Journal of cell biology* 139:1597-1610.
35. Sadoni, N., S. Langer, C. Fauth, G. Bernardi, T. Cremer, B. M. Turner, and D. Zink. 1999. Nuclear organization of mammalian genomes Polar chromosome territories build up functionally distinct higher order compartments. *The Journal of cell biology* 146:1211-1226.
36. Cremer, T., and C. Cremer. 2001. Chromosome territories, nuclear architecture and gene regulation in mammalian cells. *Nature reviews genetics* 2:292-301.
37. Shemilt, L., A. Estandarte, M. Yusuf, and I. Robinson. 2014. Scanning electron microscope studies of human metaphase chromosomes. *Philosophical Transactions of the Royal Society A: Mathematical, Physical and Engineering Sciences* 372:20130144.
38. Yusuf, M., K. Leung, K. J. Morris, and E. V. Volpi. 2013. Comprehensive cytogenomic profile of the in vitro neuronal model SH-SY5Y. *neurogenetics* 14:63-70.

## **Methodology**

### **Cell Culture and Chromosome Extraction**

Chromosomes were prepared from b-lymphocyte cells from a Yoruba cell line (GM18507), which has a normal karyotype of 46 chromosomes. This cell line was at passage four and prepared according to the protocol described in (37). The cells were cultured in a suspension of RPMI-1640 medium (Sigma Aldrich, UK) supplemented with 20% foetal bovine serum (FBS) (Sigma Aldrich, UK) and 1% L-glutamine (Sigma Aldrich, UK) at 37°C in a 5% CO<sub>2</sub> incubator. For synchronization of the cell cycle, the cells were treated with thymidine (Sigma Aldrich, UK) at a final concentration of 0.3 mg ml<sup>-1</sup> for 17 hours. To obtain chromosomes at the mitotic stage, colcemid (Invitrogen, UK) was added to the cells at a final concentration of 0.2 µg ml<sup>-1</sup>. The cells were then left for 16 hours before harvesting. This was followed by hypotonic treatment of the cells with 0.075 M potassium chloride for five minutes. Following the hypotonic treatment, the samples were fixed in three changes of 3:1 methanol: acetic acid solution.

To prepare the samples for FLIM, the chromosomes were spread on glass slides using the hanging drop method and stained with 4 µM DAPI (Invitrogen, UK) for five minutes. The glass slides were washed in a 1x phosphate buffer saline (PBS) solution (Sigma Aldrich, UK) for 5 minutes. The samples were covered with a coverslip together with deionised water as

the mounting medium.

### **Chromosome Identification using mFISH**

In order to identify the chromosomes in the samples measured with FLIM, multiplex fluorescence in-situ hybridization (mFISH) was performed using a 24XCyte mFISH probe kit (MetaSystems, Germany) following the recommended procedure of the manufacturer and according to a previously published protocol (38). The kit consists of 24 painting probes specific for the 24 different human chromosomes. Each probe is labeled with up to five different fluorophores in a combinatorial labeling format to provide 24 distinct colors. The hybridization of the probe with the DNA sites was visualized by fluorescence microscopy using a Z2 Zeiss fluorescence microscope. mFISH images were then analyzed using the ISIS software from MetaSystems.

### **FLIM Measurements**

Multiphoton fluorescence lifetime imaging of the chromosome samples was performed at the Central Laser Facility (CLF) located at the Research Complex at Harwell, UK. The custom set up has been previously described (SWB, J Microscopy, 2015, accepted for publication). Briefly, a femtosecond Ti-sapphire laser operating at 76 MHz, 200 fs pulse lengths was tuned to a wavelength of 760 nm for two-photon excitation of DAPI fluorescence. The use of multiphoton excitation here allowed for instrument response function (IRF) of less than 45 ps together with a micro-channel plate (MCP) photomultiplier tube (R3809U, Hamamatsu) as the detector. This was necessary to detect small variation in the lifetime measurements without the need for significant deconvolution of the data from the IRF. The samples were placed on a Nikon TE2000 sample stage attached to a modified Nikon EC2 confocal microscope and were raster-scanned with the laser through a x60 NA 1.2 water immersion objective. The fluorescence from the sample was collected by the same objective but bypassing the confocal optics and detected by a fast MCP-PMT detector through a short-pass filter (BG39, Comar, UK). A time-correlated single photon counting (TCSP) FLIM module (SPCM-830) from Becker & Hickl was used to record the arrival time of the photons at each x,y scan position in a time-tagging, first-in first-out (FIFO) mode.

### **Data Analysis of Lifetime Images**

The acquired fluorescence lifetime images (up to 512 x 512 pixels) were analyzed using the SPCImage software (version 4.0.6). Each pixel of the acquired images contains a

fluorescence decay function of the DAPI lifetime. The measured decay function (Eq. 1) is a convolution of the true decay function with the instrument response function (IRF). The software uses a model function (Eq. 2), which can be a single or multi-exponential function, to define the fluorescence decay function  $f(t)$  and convolutes it with the IRF. The result is compared with the measured decay function. The parameters of the model function are varied until the best fit with the measured decay function is obtained. The lifetime is then extracted from the fitted function thus resulting in an image with a lifetime value per image pixel.

$$f_m(t) = f(t) \otimes R(t - t_s) \quad (1)$$

$$f(t) = \sum_{i=1}^n a_i e^{-t/\tau_i} + a_0 \quad (2)$$

where  $f_m(t)$  is the measured fluorescence decay function,  $f(t)$  is the true fluorescence decay function,  $R$  is the instrument response function,  $t_s$  is the time shift between the response function and the fluorescence,  $a_i$  is the relative amplitude of the exponential component  $i$ ,  $\tau_i$  is the lifetime of the exponential component  $i$ , and  $a_0$  is a constant offset-correction.

## Tables

**Table 1.** Lifetime values for the heteromorphous regions.

Chromosome #	Mean Lifetime $\pm$ SD, ns
1	2.58 $\pm$ 0.06
9a	2.38 $\pm$ 0.06
9b	2.21 $\pm$ 0.05
15	2.43 $\pm$ 0.05
16	2.55 $\pm$ 0.06
Y	2.58 $\pm$ 0.03

**Table 2.** Quantitative analysis of the heterochromatic blocks.

Block #	Volume, $\mu\text{m}^3$	Distance*/Radius of Nucleus	Mean Lifetime $\pm$ SD, ns
1	8.04	0.91	2.58 $\pm$ 0.08
2	8.83	0.84	2.54 $\pm$ 0.06
3	0.16	0.77	2.44 $\pm$ 0.03
4	0.63	0.71	2.21 $\pm$ 0.03
5	0.17	0.61	2.45 $\pm$ 0.03
6	0.80	0.59	2.28 $\pm$ 0.03
7	1.90	0.54	2.56 $\pm$ 0.04
8	6.14	0.48	2.55 $\pm$ 0.05
9	5.22	0.47	2.54 $\pm$ 0.06

\*The distance corresponds to that between the center of mass (COM) of the nucleus and the COM of the heterochromatic blocks.

## Figures

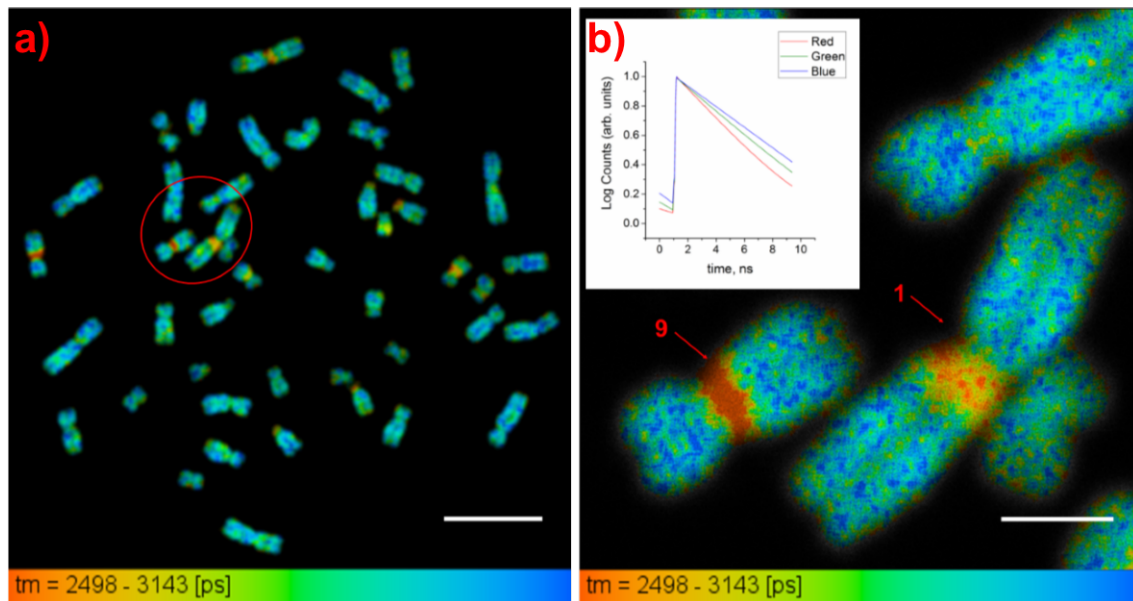


**Figure 1.** Variations in DAPI lifetime along the length of the chromosomes. Lifetime images of a) a chromosome spread (scale bar = 10  $\mu\text{m}$ ) and b) an expanded image of the encircled region in Figure 1a taken at a higher pixel resolution showing chromosomes 1 and 9 (scale bar = 2  $\mu\text{m}$ ). Figure 1b inset: normalized DAPI fluorescence decay curves at selected pixels from the red, green, and blue regions in chromosome 9 in Figure 1b. The range of the lifetime color scale runs from 2.50 ns (red) to 3.14 ns (blue), as shown.

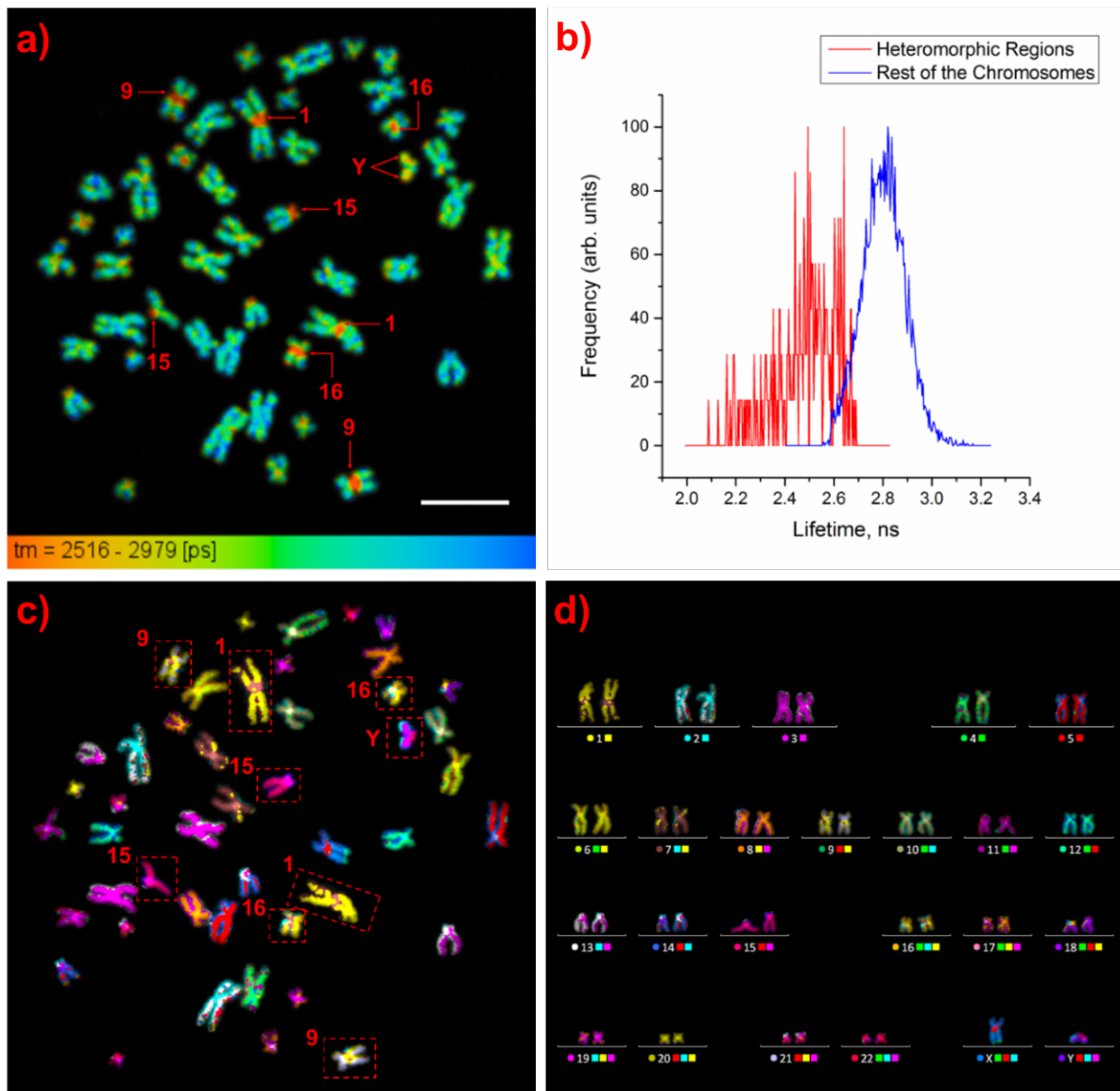


**Figure 2.** Identification of heteromorphous regions in chromosomes. a) Lifetime image of a chromosome spread with arrows showing the heteromorphous regions (scale bar = 10  $\mu$ m) b) Normalized lifetime distribution curves for the heteromorphous regions and the rest of the chromosomes showing shorter DAPI lifetimes in the heteromorphous regions than in the rest of the chromosomes. c) mFISH image of the measured chromosome spread. d) Karyotyping of the chromosomes in Figures 2a and c based on color.

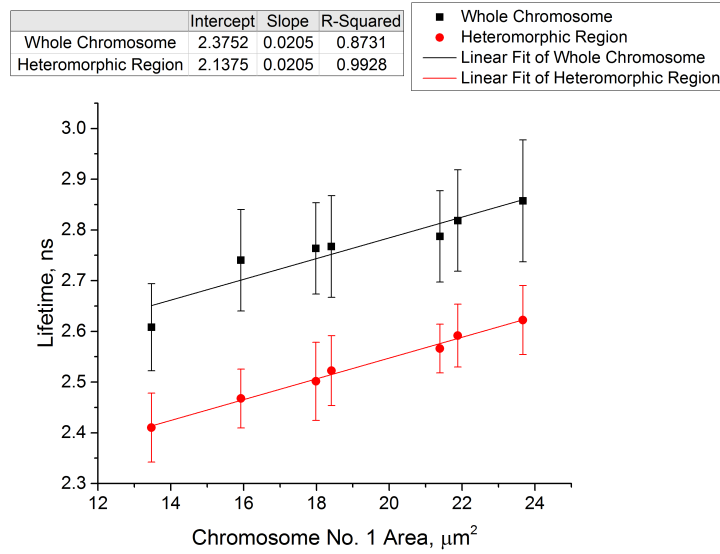


**Figure 3.** Mean fluorescence lifetime of DAPI for various chromosome 1's and their heteromorphic regions plotted against the area of the chromosomes. The error bars represent the standard deviation. Thus, DAPI is sensitive to both general chromosome length compactions as well as localized sub-chromosome condensation.

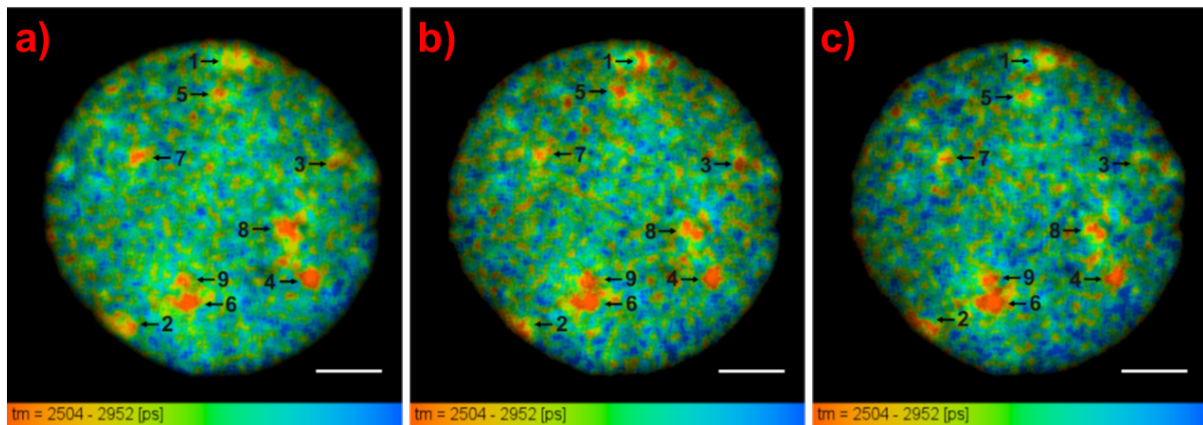


**Figure 4.** Selected focal planes from the z-stack of the lifetime images of a nucleus at a) -0.50  $\mu\text{m}$ , b) 0  $\mu\text{m}$ , and c) +0.50  $\mu\text{m}$  focus (scale bars = 5  $\mu\text{m}$ , see Supplementary Fig. 3 for all the focal planes in the z-stack).